AIAA JOURNAL
Vol. 33, No. 5, May 1995

Buckling of Arbitrary Quadrilateral Anisotropic Plates

Navin Jaunky* and N. F. Knight Jr.†
Old Dominion University, Norfolk, Virginia 23529-0247
and
D. R. Ambur‡
NASA Langley Research Center, Hampton, Virginia 23681

The problem of buckling of arbitrary quadrilateral anisotropic plates with different boundary conditions under combined in-plane loading is considered. A Rayleigh–Ritz method combined with a variational formulation and a first-order transverse-shear-deformation theory is used. The Ritz functions consist of polynomials which include "circulation" functions that impose various boundary conditions. Numerical results are obtained for isotropic, orthotropic, and anisotropic plates with skewed geometries and are compared with existing results that use series solutions and with results generated from finite element simulations.

Nomenclature

a_{ij}	= jth coefficient of ith component of displacement vector
D_i	= ith component of displacement vector
$\boldsymbol{E}_p, \boldsymbol{E}_c$	= matrices defined by Eq. (8)
$\boldsymbol{J}$	= Jacobian matrix
K	= buckling coefficients, Eqs. (17–19)
$\boldsymbol{k}_{gij}$	= geometric stiffness matrix, Eq. (14)
$\boldsymbol{k}_{ij}$	= linear stiffness matrix, Eq. (13)
N_i	= bilinear shape function
$\bar{N}_x$	= axial prestress
$\bar{N}_{xy}$	= shear prestress
$\bar{N}_y$	= transverse prestress
q_i	= generalized degrees of freedom
$\boldsymbol{T}$	= matrix defined by Eq. (8)
α_{jk}	= orthogonalizing coefficient, Eq. (4)
Γ_i	= circulation function, Eq. (3)
$\boldsymbol{\Theta}_j$	= matrix defined by Eq. (10)
λ	= eigenvalue or critical load factor
ξ, η	= natural coordinate system
ψ	= plate skew angle

Introduction

A SIGNIFICANT impact on aircraft performance and structural cost can be made by using composite materials for aircraft primary structures. Such applications of composite materials are expected to result in a 30–40% weight savings and a 10–30% cost reduction compared to conventional metallic structures. Realization of these goals requires the integration of innovative structural concepts, high-performance composite materials, and low-cost manufacturing processes. A structural concept that has the potential to satisfy these requirements is the family of continuous-filament, grid-stiffened structures which can be manufactured by automated processes to produce wing and fuselage structures. The stiffener pattern and, hence, the geometry of the skin segments for these structural applications is primary determined by the combination of in-plane axial and shear loading experienced by the structure. In the case of a diagonal stiffener configuration, for example, the skin segments have a rhombic geometry. Even for the case of a more conventional orthogonal stiffener pattern used for a swept-back wing shown in Fig. 1, the skin geometry segments have a skewed quadrilateral geometry. Skewed and rhombic plates also result when exploiting structural tailoring characteristics of composite materials.[1] For these applications, stiffener pattern and stiffness determine the type of boundary conditions imposed on the edges of structural skin segments. Therefore, an analysis method for composite skin segment buckling should be general enough to include different boundary conditions, combined in-plane loading conditions, an arbitrary quadrilateral geometry, and anisotropic material properties. An analytical tool with these capabilities is needed for the preliminary design of stiffened structures.[2,3]

A review of the existing literature indicates that some aspects of buckling of arbitrary quadrilateral plates have been addressed, but mostly for skewed isotropic plates using classical laminated plate theory (CLPT). A thorough review of the literature for buckling of skewed plates with simply supported and clamped boundary conditions using CLPT and the Rayleigh–Ritz method is presented in Ref. 4, which also compares the results published by different authors. None of the references cited in Ref. 4 or other recent publications (e.g., Refs. 5 and 6) in the open literature address the buckling of skewed or rhombic anisotropic plates with or without transverse-shear-deformation effects. The present paper describes an analysis method for skewed and rhombic anisotropic plates that includes transverse-shear-deformation effects and presents results for skewed isotropic, orthotropic, and anisotropic plates subjected to different boundary conditions and in-plane loading conditions.

Analytical Approach

The analytical approach for the present study makes use of the principle of minimum total potential energy and a Rayleigh–Ritz approach based on a high-order complete polynomial functions. These polynomial functions are expressed in terms of a set of natural coordinates for quadrilateral plate rather than the usual rectangular Cartesian coordinates. This approach makes use of a finite element concept for mapping the arbitrary quadrilateral geometry to a square geometry in natural-coordinate space. The physical domain $(x–y)$ is transformed into a computational domain $(\xi–\eta)$ where the displacements and rotations of the plate are approximated by selected polynomials. The Jacobian of the transformation is used to relate derivatives in the two domains. Finally, a variational method is used to develop an eigenvalue problem for determining the critical load.

Mapping and Ritz Function

Consider an arbitrary quadrilateral plate subjected to a state of combined in-plane loading as shown in Fig. 2, where the loading and the material properties are defined using the coordinate system shown. The physical domain $(x–y)$ is transformed as into a

Received July 22, 1994; revision received Dec. 19, 1994; accepted for publication Jan. 7, 1995. Copyright © 1995 by the American Institute of Aeronautics and Astronautics, Inc. All rights reserved.

*Graduate Research Assistant, Aerospace Engineering Department.
†Associate Professor, Aerospace Engineering Department. Senior Member AIAA.
‡Senior Aerospace Engineer, Structural Mechanics Branch, Structures Division. Senior Member AIAA.

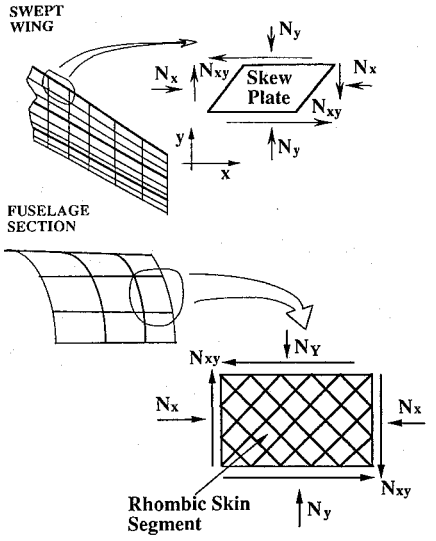

Fig. 1 Wing and fuselage sections, showing skin segment geometry between stiffeners.

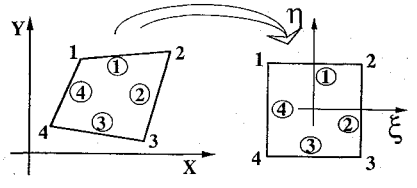

Fig. 2 Physical domain (left) and computational domain (right).

computational domain defined by a ξ–η natural coordinate system by the following transformation:

$$x(\xi,\eta)=\sum_{i=1}^{4}N_i(\xi,\eta)x_i$$
$$y(\xi,\eta)=\sum_{i=1}^{4}N_i(\xi,\eta)y_i \tag{1}$$

where N_i are the standard bilinear Lagrangian shape functions from the finite element method, and x_i and y_i are the physical coordinates of the ith corner of the plate. That is, the geometry of the plate is represented as a general quadrilateral with straight edges. Transformation of the physical domain to a computational domain is necessary so that boundary conditions can be imposed easily. The Jacobian of the transformation is

$$\boldsymbol{J}=\begin{bmatrix}\dfrac{\partial x}{\partial\xi} & \dfrac{\partial y}{\partial\xi}\\[2ex] \dfrac{\partial x}{\partial\eta} & \dfrac{\partial y}{\partial\eta}\end{bmatrix} \tag{2}$$

which is independent of the natural coordinates for general parallelogram-shaped geometries. (Note that the transpose of Eq. (2) was used in the computations of the results presented in Ref. 7, which lead to numerical errors.)

A first-order shear-deformation theory (FSDT) is used in the analysis and, thus, the displacement field has five independent components. The components of the displacement vector are three translations (D_1, D_2, $D_3 = u, v, w$) and two bending rotations (D_4, $D_5 = \phi_x, \phi_y$). Each displacement component is then approximated independently by different Ritz functions. The approximation for the ith component of the displacement vector is

$$D_i=\sum_{j=1}^{N}a_{ij}d_{ij}(\xi,\eta)\qquad i=1,2,3,4,5 \tag{3}$$

where

$$d_{ij}=\Gamma_i(\xi,\eta)\xi^{m_j}\eta^{n_j}$$
$$\Gamma_i(\xi,\eta)=(1-\eta)^{p_i}(1-\xi)^{q_i}(1+\eta)^{r_i}(1+\xi)^{s_i}$$
$$m_j,n_j=(0,0),(1,0),(0,1),(2,0),(1,1),(0,2)$$
$$(3,0),(2,1),(1,2),(0,3),\ldots$$

where d_{ij} represents the jth polynomial term in the N-term approximation for the ith displacement component and a_{ij} are unknown coefficients to be determined. The values of m_j and n_j are used basically to identify terms in the two-dimensional Pascal's triangle. The number of terms N defines the order of a complete function in two variables.

The term $\Gamma_i(\xi,\eta)$ in Eq. (3) is the "circulation" function used to impose different boundary conditions. It is the product of four linear functions of the natural coordinates wherein each function will take on a zero value along at least one edge [e.g., the function $(1-\eta)$ will have zero value on edge 1 where $\eta=1$]. The subscript i refers to the ith displacement component and ranges in value from one to five corresponding to the displacement components u, v, w, ϕ_x, and ϕ_y, respectively. Each of the four linear functions is raised to an independent exponent for each displacement component (i.e., p_i refers to edge 1, q_i refers to edge 2, r_i refers to edge 3, and s_i refers to edge 4). If the ith displacement component is unrestrained or free on a given edge, then the exponent for that edge will have a value of zero. If the ith displacement component is restrained or fixed on a given edge, the exponent for that edge will have a value of one. For example, the displacement field v can be defined as free on edge 1 and fixed on the remaining edges by specifying $p_2=0$, $q_2=1$, $r_2=1$, and $s_2=1$. Only geometric boundary conditions are imposed in this approach. Thus, a simply supported condition for bending fields can be imposed on edge 1 by setting $p_3=1$ for w, $p_4=p_5=0$ for ϕ_x and ϕ_y. A clamped condition for bending fields can be imposed on edge 1 by setting $p_3=p_4=p_5=1$ for w, ϕ_x, and ϕ_y. A free-edge condition can be imposed on edge 1 by setting $p_i=0$ for $i=1,2,3,4,5$ for u, v, w, ϕ_x, and ϕ_y.

Similar Ritz functions were used in Ref. 8 to determine the transverse vibration response of triangular plates where characteristic orthogonal polynomials are generated by the Gram–Schmidt process. The Gram–Schmidt process can be summarized as follows. Let

$$d_i=\sum_{j=1}^{N}a_{ij}\Phi_j \tag{4}$$

where

$$\Phi_j=\Gamma_{ij}-\sum_{k=1}^{j-1}\alpha_{jk}\Phi_k$$

then

$$\Gamma_{i1}=\Gamma_{i1}(\xi,\eta),\qquad \Gamma_{ij}=\Gamma_{i1}(\xi,\eta)\xi^{m_j}\eta^{n_j}$$

and

$$\alpha_{jk}=\int\int_A\Gamma_{ij}\Phi_k\,dA\Big/\int\int_A\Phi_k\Phi_k\,dA,\qquad k=1,\ldots,(j-1)$$

Orthogonal characteristic polynomials ensure good convergence. Also the use of orthogonal characteristic polynomials significantly increases the computing time needed to evaluate the linear stiffness and geometric stiffness matrices. However, in the present method nearly all of the orthogonalizing coefficients (α_{jk}) corresponding to a circulation function (Γ_i) as defined by Eq. (3) are equal to zero. Therefore, the orthogonalization is not performed in the present method, and it appears to only have a negligible effect on convergence.

Variational Statement and Rayleigh–Ritz Method

An N-term approximation for each component of the displacement field can be written in a matrix form as

$$\begin{Bmatrix} u \\ v \\ w \\ \phi_x \\ \phi_y \end{Bmatrix} = \sum_{j=1}^{N} \begin{bmatrix} d_{1j} & 0 & 0 & 0 & 0 \\ 0 & d_{2j} & 0 & 0 & 0 \\ 0 & 0 & d_{3j} & 0 & 0 \\ 0 & 0 & 0 & d_{4j} & 0 \\ 0 & 0 & 0 & 0 & d_{5j} \end{bmatrix} \begin{Bmatrix} a_{1j} \\ a_{2j} \\ a_{3j} \\ a_{4j} \\ a_{5j} \end{Bmatrix} \tag{5}$$

or

$$D = \sum_{j=1}^{N} S_j q_j$$

The strain-displacement relations according to a first-order shear-deformation theory are

$$\begin{aligned} \epsilon_x &= u_{,x} + z\phi_{x,x} = \epsilon_x^0 + z\kappa_x \\ \epsilon_y &= v_{,y} + z\phi_{y,y} = \epsilon_y^0 + z\kappa_y \\ \epsilon_z &= w_{,z} = 0 \\ \gamma_{xy} &= u_{,y} + v_{,x} + z(\phi_{y,x} + \phi_{x,y}) = \gamma_{xy}^0 + z\kappa_{xy} \\ \gamma_{xz} &= u_{,z} + w_{,x} = \phi_x + w_{,x} \\ \gamma_{yz} &= v_{,z} + w_{,y} = \phi_y + w_{,y} \end{aligned} \tag{6}$$

where a comma indicates differentiation with respect to the subscripted variable. The midplane strains and curvature are defined in a matrix form as

$$\begin{Bmatrix} \epsilon_x^0 \\ \epsilon_y^0 \\ \gamma_{xy}^0 \\ \kappa_x \\ \kappa_y \\ \kappa_{xy} \\ \gamma_{xz} \\ \gamma_{yz} \end{Bmatrix} = \begin{bmatrix} \partial_x & 0 & 0 & 0 & 0 \\ 0 & \partial_y & 0 & 0 & 0 \\ \partial_y & \partial_x & 0 & 0 & 0 \\ 0 & 0 & 0 & \partial_x & 0 \\ 0 & 0 & 0 & 0 & \partial_y \\ 0 & 0 & 0 & \partial_y & \partial_x \\ 0 & 0 & \partial_x & 1 & 0 \\ 0 & 0 & \partial_y & 0 & 1 \end{bmatrix} \begin{Bmatrix} u \\ v \\ w \\ \phi_x \\ \phi_y \end{Bmatrix} \tag{7}$$

or

$$E_p = LD$$

where $\partial_x = \partial/\partial_x$ and $\partial_y = \partial/\partial_y$. The differential operators in matrix L have to be expressed in terms of the natural coordinate system. Using Eqs. (5) and (7), the midplane strains and curvatures can be written in terms of generalized degrees of freedom as

$$E_p = TE_c = T\sum_{j=1}^{N} \Theta_j q_j \tag{8}$$

where subscripts p and c denote physical and computational, respectively, T is a 8×12 matrix consisting of the elements of the inverse of the Jacobian, and E_c is a column vector consisting of the Ritz functions and their derivatives. For example, E_p^κ, E_c^κ and T^κ for the curvatures only are

$$\begin{Bmatrix} \kappa_x \\ \kappa_y \\ \kappa_{xy} \end{Bmatrix} = \begin{bmatrix} \dfrac{\partial\xi}{\partial x} & \dfrac{\partial\eta}{\partial x} & 0 & 0 \\ 0 & 0 & \dfrac{\partial\xi}{\partial y} & \dfrac{\partial\eta}{\partial y} \\ \dfrac{\partial\xi}{\partial y} & \dfrac{\partial\eta}{\partial y} & \dfrac{\partial\xi}{\partial x} & \dfrac{\partial\eta}{\partial x} \end{bmatrix} \begin{Bmatrix} \dfrac{\partial\phi_x}{\partial\xi} \\ \dfrac{\partial\phi_x}{\partial\eta} \\ \dfrac{\partial\phi_y}{\partial\xi} \\ \dfrac{\partial\phi_y}{\partial\eta} \end{Bmatrix} \tag{9}$$

or

$$E_p^\kappa = T^\kappa E_c^\kappa$$

and Θ_j for the rotations ϕ_x and ϕ_y is developed from

$$E_c^\kappa = \sum_{j=1}^{N} \begin{bmatrix} \dfrac{\partial d_{4j}}{\partial\xi} & 0 \\ \dfrac{\partial d_{4j}}{\partial\eta} & 0 \\ 0 & \dfrac{\partial d_{5j}}{\partial\xi} \\ 0 & \dfrac{\partial d_{5j}}{\partial\eta} \end{bmatrix} \begin{Bmatrix} a_{4j} \\ a_{5j} \end{Bmatrix} = \sum_{j=1}^{N} \Theta_j^\kappa q_j^\kappa \tag{10}$$

The matrices T, E_c, and Θ_j can be written for all midplane strains and curvatures in a similar manner.

The strain energy of the plate is given by

$$U_e = \frac{1}{2}\int_A \left(N_x\epsilon_x^0 + N_y\epsilon_y^0 + N_{xy}\gamma_{xy}^0 + M_x\kappa_x + M_y\kappa_y + M_{xy}\kappa_{xy} + Q_x\gamma_{xz} + Q_y\gamma_{yz}\right) \mathrm{d}A \tag{11}$$

or

$$U_e = \frac{1}{2}\int_A F^T E_p \,\mathrm{d}A$$

and

$$F = QE_p$$

where F is a column vector consisting of in-plane and transverse force and moment resultants, and Q is an 8×8 constitutive matrix given by

$$Q = \begin{bmatrix} [A]_{3\times3} & [B]_{3\times3} & [0]_{3\times2} \\ [B]_{3\times3} & [D]_{3\times3} & [0]_{3\times2} \\ [0]_{2\times3} & [0]_{2\times3} & [C]_{2\times2} \end{bmatrix} \tag{12}$$

with A_{ij}, B_{ij}, D_{ij}, and C_{rs} being the extensional, coupling, bending, and transverse shear stiffness matrices of the plate. From Eq. (11), the expression for the strain energy can be rewritten as

$$U_e = \frac{1}{2}\int_A E_c^T T^T Q T E_c^T \,\mathrm{d}A = \frac{1}{2}\sum_{i=1}^{N}\sum_{j=1}^{N} q_i^T k_{ij} q_j \tag{13}$$

where k_{ij} is the linear stiffness matrix given by

$$k_{ij} = \int_{-1}^{1}\int_{-1}^{1} \Theta_i^T T^T Q T \Theta_j |J| \,\mathrm{d}\xi \,\mathrm{d}\eta$$

and $|J|$ is the determinant of the Jacobian matrix.

The work done by the applied in-plane prestress is developed in a way similar to the stiffness matrix and is given by

$$\begin{aligned} W_d &= \frac{\lambda}{2}\int_A [w_{,x} w_{,y}] \begin{bmatrix} \bar{N}_x & \bar{N}_{xy} \\ \bar{N}_{xy} & \bar{N}_y \end{bmatrix} \begin{Bmatrix} w_{,x} \\ w_{,y} \end{Bmatrix} \mathrm{d}A \\ &= \frac{\lambda}{2}\sum_{i=1}^{N}\sum_{j=1}^{N} q_i^T \begin{bmatrix} 0 & 0 & 0 & 0 & 0 \\ 0 & 0 & 0 & 0 & 0 \\ 0 & 0 & g_{ij} & 0 & 0 \\ 0 & 0 & 0 & 0 & 0 \\ 0 & 0 & 0 & 0 & 0 \end{bmatrix} q_j \\ &= \frac{\lambda}{2}\sum_{i=1}^{N}\sum_{j=1}^{N} q_i^T k_{gij} q_j \end{aligned} \tag{14}$$

where k_{gij} is the geometric stiffness matrix, $\bar{N}_x$, $\bar{N}_y$, $\bar{N}_{xy}$ denote the in-plane prestress state, and λ denotes the critical load factor or eigenvalue.

Evaluation of the linear stiffness matrix coefficients k_{ij} and geometric stiffness coefficients k_{gij} requires integration over the plate geometry as indicated by Eqs. (13) and (14). Since higher order polynomial approximations are used for the displacement fields, the integrands will also involve higher order polynomial terms which will require a large number of Gaussian quadrature points for exact numerical integration. However, if the plate geometry is restricted to parallelogram-shaped domains, the Jacobian matrix will be independent of the natural coordinates of the computational domain. For this case, integration can be carried out analytically by utilizing symbolic computational results rather than numerical integration which results in significant savings in computational time.

The critical loading is determined from an analysis based on a criterion that during buckling, the elastic energy stored in the structure is equal to the work done by the applied loading during bending.[9] The total potential energy of the system in terms of the Rayleigh–Ritz unknown coefficients is given by

$$\Pi = \frac{1}{2}\sum_{i=1}^{N}\sum_{j=1}^{N} q_i^T k_{ij} q_j - \frac{\lambda}{2}\sum_{i=1}^{N}\sum_{j=1}^{N} q_i^T k_{gij} q_j \qquad (15)$$

Imposing the stationary conditions with respect to q_i gives

$$\sum_{i=1}^{N}\sum_{j=1}^{N}(k_{ij} - \lambda k_{gij})q_j = 0 \qquad (16)$$

where the critical load factor (λ) and the corresponding mode shape (Σq_j) from Eq. (16) can be obtained by the use of an eigensolver.

Numerical Results and Discussion

Numerical results are presented for the buckling analyses of skewed plates. Isotropic, orthotropic, and anisotropic plates with different boundary conditions are considered. The present formulation is based on the principle of minimum total potential energy which slightly overpredicts results compared to values from exact solutions. Also the present formulation does not introduce any geometric distortion for cases considered since the mapping between the physical and computational domains does not introduce any errors. For simply supported conditions, only geometric boundary conditions are prescribed, and since transverse shear deformations are included, the rotations are independent of the out-of-plane deflection. Results from the present analysis were obtained using a larger number of terms than necessary for obtaining converged solutions. These results are compared with existing solutions and with results generated from finite element analyses.

Finite element results are obtained using STAGS.[10] The STAGS finite element analyses were carried out using a 30 × 30 mesh of C^1 4-node elements. More refined finite element meshes were considered and gave the same solutions as the 30 × 30 mesh. In these studies, the prebuckling stress state was prescribed to be uniform and, hence, the linear static solution is avoided and a precise prestress state is defined. In the STAGS models, the simply supported boundary conditions along the skewed edges are only established approximately; that is, only the out-of-plane deflection is equal to zero whereas the moment is not prescribed. An additional consideration for the finite element solutions for plate geometries with a nonzero skew angle is the susceptibility of the results to element distortion. Mesh distortion is known to affect the linear stress solution (e.g., Ref. 11), and this behavior may also affect the buckling analyses. The finite element solutions may become increasingly susceptible to mesh distortion effects as the skew angle ψ increases.

Simulations are also made using VICON[12] wherein a semi-infinite plate is analyzed using complex Fourier series with constraints imposed at points along user-defined lines across the width at regular intervals to simulate a finite plate. In the VICON models, the simply supported boundary condition is only satisfied approximately along skewed edges, whereas along horizontal edges the simply supported boundary condition is satisfied exactly. As such the VICON models for skewed plates with simply supported boundary conditions represent a plate which is continuous over the supports as would occur in an array of skewed panels and not for moment-free edges. Hence, the VICON models do not exactly represent a finite plate but approximate it depending on the number and type of constraint points and modes. For all VICON analyses, 10 modes and 10 constraint points were used. The VICON results converged from above for increasing number of constraint modes and from below for increasing number of constraint points.

Table 1 Buckling coefficient K for simply supported isotropic plates, $a/b = 1$

	$\psi = 0$ deg	$\psi = 15$ deg	$\psi = 30$ deg	$\psi = 45$ deg
Mizusawa et al.[18]	4.000	3.778	3.160	2.160
Wang et al.[4]	4.000	3.860	3.480	2.650
Kitipornchai et al.[15]	4.000	3.825	3.331	2.526
VICON	4.000	4.126	4.250	3.387
STAGS	4.003	3.825	3.288	2.426
Present analysis	3.999	3.832	3.380	2.709[a]

[a]Using 91 terms, present analysis gives 2.630.

Table 2 Buckling coefficient K for clamped isotropic plates, $a/b = 1$

	$\psi = 0$ deg	$\psi = 15$ deg	$\psi = 30$ deg	$\psi = 45$ deg
Wittrick[13]	10.080	—	7.670	5.410
Durvasula[14]	10.080	9.462	7.639	5.110
Wang et al.[4]	10.080	9.479	7.734	5.170
Kitipornchai et al.[15]	10.074	9.431	7.615	5.028
VICON	10.070	9.445	7.639	5.025
STAGS	10.081	9.416	7.579	4.980
Present analysis	10.073	9.432	7.621	5.154[a]

[a]Using 91 terms, present analysis gives 5.051.

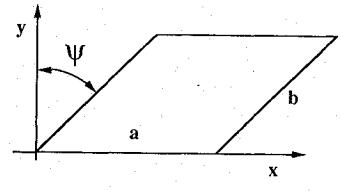

Fig. 3 Skewed plate geometry.

In the following sections, analytical results are presented for four categories of problems. The first set of problems involves skewed isotropic plates with simply supported and clamped boundary conditions subjected to axial compression, which were originally addressed by Wittrick.[13] The second set of problems involves skewed orthotropic plates subjected to combined loading with simply supported boundary conditions. The third set of problems involves skewed anisotropic plates subjected to combined loading with various boundary conditions. Finally the effect of transverse shear deformation is studied for isotropic and anisotropic skewed plates.

Isotropic Plates under Uniaxial Loading

The buckling of clamped and simply supported isotropic skewed plate has been studied by many researchers (e.g., see Refs. 4 and 13–18). Of these references, only Kitipornchai et al.[15] considered transverse shear deformations using a first-order shear-deformation theory. Results from the present analysis are presented and compared with existing results in Tables 1 and 2. Results obtained using the STAGS finite element code and VICON are also presented. Results are nondimensionalized and presented as a buckling coefficient defined as

$$K = \left(N_{cr} b^2 \cos^4\psi / \pi^2 D_{22}\right) \qquad (17)$$

where N_{cr} is the critical load, b the width of the plate, ψ the skew angle (see Fig. 3), and D_{22} the transverse bending stiffness from classical laminated plate theory. Results given in Tables 1 and 2 are

for cases with all edges simply supported and all edges clamped, respectively, with an aspect ratio (a/b) of 1.0 and a thickness-to-width ratio (t/b) of 0.001. Results from the present analysis were obtained using a 66-term series solution (complete 10th-order polynomial per degree of freedom).

Results shown in Table 1 for simply supported plates indicate that all solution methods are in excellent agreement for the rectangular plate geometry case (0-deg skew angle). In all cases, the buckling mode shape has one half-wave in each direction. The analyses of Wang et al.[4] and Kitipornchai et al.[15] are essentially identical except that the latter study included transverse shear deformation. As such, the results from Ref. 15 are slightly lower in value than those of Ref. 4. However, these plates are very thin and transverse-shear-deformation effects should be negligible. The results from the present formulation correlate very well with the results presented by Wang et al.[4] and Kitipornchai et al.[15] Those presented by Mizusawa et al.[18] are below that of the present analyses and any other results shown. The STAGS finite element results follow the results of the present formulation, but mesh distortion appears to influence the results as the skew angle increases. The VICON results are much higher in value than any other results except for the 0-deg skew angle case. The differences for nonzero-deg skew angle is due to the fact that the constraints on the skewed edges satisfy only the geometric boundary conditions.

Results shown in Table 2 for the clamped plates indicate that the present approach gives buckling coefficients that are in good agreement with the other results. In all cases, the buckling mode has one half-wave in each direction. The VICON results for these cases are very close to the other results since clamped boundary conditions can be approximated easily along the skew edges. The STAGS analyses seem to be affected less by mesh distortion for clamped boundary conditions than for simply supported boundary conditions.

Orthotropic Plates Under Combined Loading

In this section, results are presented for orthotropic skewed plates with ratios $a/b = 1$ and $t/b = 0.001$. The boundary conditions considered are all edges simply supported. Four load cases are also considered for each set of boundary conditions.

Load case A:

$$N_x = 1, \qquad N_y = N_{xy} = 0$$

Load case B:

$$N_x = N_y = 1, \qquad N_{xy} = -0.5$$

Load case C:

$$N_x = N_y = 1, \qquad N_{xy} = 0$$

Load case D:

$$N_x = N_y = 1, \qquad N_{xy} = 0.5$$

Load case A corresponds to uniaxial compression; load case C corresponds to biaxial compression; and load cases B and D correspond to combined loading with negative and positive in-plane shear. These analysis results are presented in subsequent tables as a nondimensional buckling coefficient K given by

$$K = \left(\lambda_{cr} b^2/\pi^2 D_{22}\right) \tag{18}$$

where λ_{cr} is the critical eigenvalue and b is the width of the plate as shown in Fig. 3. Results from the present analysis were obtained using a 78-term series (complete 11th-order polynomials). Results generated from STAGS and VICON are also presented and compared.

Orthotropic skewed plates with all edges simply supported and subjected to combined loading were also treated by Kennedy and Prabhakara,[19] using the Galerkin method with Fourier series terms as Ritz functions to solve the stability equations for thin plates. The series solution satisfied the natural boundary conditions, whereas the remaining boundary conditions are satisfied indirectly by a procedure given by Green.[20] A similar formulation used by Phillips and Gurdal[3] for buckling of orthotropic rhombic plates concluded that the solution from such a formulation converged from below. Kennedy and Prabhakara[19] used a 9-term series in their solution, whereas Phillips and Gurdal used a 20-term series which they showed to represent a converged solution. However, since Phillips and Gurdal[3] did not consider a variety of cases considered by Kennedy and Prabhakara,[19] results obtained from the present analysis are compared with those of Ref. 19 for cases with $D_{11}/D_{22} = 1$ and $D_{11}/D_{22} = 5$ in Tables 3 and 4, respectively. For both cases, $D_{66}/D_{22} = 0.5$ and the major Poisson's ratio $\nu_{12} = 0.25$.

Comparison between results from Kennedy and Prabhakara[19] and those from the present formulation is very good for the case of $\psi = 15$ deg and deviate as the skew angle increases. However, based on similar results in Ref. 3, the results from Ref. 19 converged from below and may not have completely converged. Comparison between finite element results and those of the present formulation is good with small differences occurring as the skew angle increases. A contributing factor to these differences is the increasing mesh distortion in the finite element models which in linear static analyses is known to cause a reduction in stiffness for this STAGS 4-node element. The buckling coefficients predicted by VICON are all higher than any other results because of the manner in which the simply supported boundary conditions are imposed on the skewed edges. Finally, the sign of the in-plane shear prestress has a significant effect on the buckling coefficient for skewed plates, and the effect increases as the degree of orthotropy increases. Also the differences between the results of the present formulation and those of STAGS

Table 3 Buckling coefficient K for simply supported skewed plates, $a/b = 1, D_{11}/D_{22} = 1$

Load case	Kennedy and Prabhakara[19]	VICON	STAGS	Present analysis
		$\psi = 15$ deg		
A	——	4.739	4.770	4.773
B	2.150	2.186	2.114	2.116
C	2.340	2.435	2.296	2.298
D	2.490	2.707	2.452	2.454
		$\psi = 30$ deg		
A	——	7.555	6.217	6.356
B	2.300	2.775	2.340	2.383
C	2.640	3.333	2.677	2.730
D	3.020	4.009	3.054	3.121
		$\psi = 45$ deg		
A	——	13.548	10.108	11.043
B	2.900	4.412	3.119	3.342
C	3.380	5.368	3.656	3.938
D	4.000	6.732	4.334	4.697

Table 4 Buckling coefficient K for simply supported skewed plates, $a/b = 1, D_{11}/D_{22} = 5$

Load case	Kennedy and Prabhakara[19]	VICON	STAGS	Present analysis
		$\psi = 15$ deg		
A	——	9.295	9.122	9.131
B	3.860	3.875	3.883	3.888
C	4.290	4.353	4.319	4.324
D	4.730	4.922	4.759	4.763
		$\psi = 30$ deg		
A	——	13.750	11.601	11.700
B	3.810	4.317	3.930	3.962
C	4.480	5.220	4.654	4.693
D	5.440	6.550	5.613	5.661
		$\psi = 45$ deg		
A	——	25.170	18.606	19.269
B	4.350	5.440	4.649	4.787
C	5.260	6.740	5.626	5.802
D	6.500	8.800	7.060	7.296

Table 5 Buckling coefficient K for simply supported anisotropic skewed plates $[\pm 45/90/0]_s$ laminate

Load case	VICON	STAGS	Present analysis
		$\psi = 30$ deg	
B	2.725	2.373	2.396
C	3.269	2.758	2.787
D	4.017	3.227	3.264
		$\psi = 45$ deg	
B	4.153	3.001	3.155
C	5.070	3.553	3.749
D	6.415	4.286	4.545

Table 6 Buckling coefficient K for simply supported anisotropic skewed plates $[45/90/-45]_s$ laminate

Load case	VICON	STAGS	Present analysis
		$\psi = 30$ deg	
B	1.552	1.484	1.4887
C	1.870	1.764	1.769
D	2.321	2.139	2.144
		$\psi = 45$ deg	
B	2.510	2.023	2.106
C	3.040	2.419	2.523
D	3.800	2.969	3.105

Table 7 Buckling coefficient K for simply supported-clamped anisotropic skewed plates $[\pm 45/90/0]_s$ laminate

Load case	VICON	STAGS	Present analysis
		$\psi = 30$ deg	
B	4.170	4.130	4.158
C	4.901	4.850	4.884
D	5.718	5.644	5.685
		$\psi = 45$ deg	
B	5.791	5.722	5.849
C	6.990	6.917	7.085
D	8.512	8.455	8.688

for $D_{11}/D_{22} = 1$ are approximately 8% for $\psi = 45$ deg whereas those for $D_{11}/D_{22} = 5$ are approximately 3% for $\psi = 45$ deg. This suggests errors due to mesh distortion are compensated in some way due to the presence of material orthotropy.

Anisotropic Plates Under Combined Loading

Anisotropic skewed plates with an aspect ratio (a/b) of 1, a thickness-width ratio (t/b) of 0.001, and two laminate stacking sequences are considered here. Laminates 1 and 2 have ply stacking sequences of $[\pm 45/90/0]_s$ and $[45/90/-45]_s$, respectively. The ply elastic constants are $E_{11} = 24.5$ Msi, $E_{22} = 1.64$ Msi, $G_{12} = G_{13} = G_{23} = 0.87$ Msi, $\nu_{12} = 0.3$. The degree of anisotropy for these laminates is indicated by the magnitude of the bending-twisting terms (D_{16} or D_{26}) relative to the magnitude of the bending stiffness terms (D_{11} or D_{22}). For laminate 2 the ratio D_{26}/D_{22} is approximately three times the ratio of D_{16}/D_{11} for laminate 1. The results are presented as a nondimensional buckling coefficient K given by Eq. (18).

Results for anisotropic skewed plates obtained using a 78-term series solution are given in Tables 5 and 6 for all edges simply supported, in Tables 7 and 8 for the horizontal edges simply supported and skewed edges clamped, and in Tables 9 and 10 for all edges clamped. The results in Tables 5, 7, and 9 are for laminate 1 and those in Tables 6, 8, and 10 are for laminate 2. For simply supported boundary conditions, the VICON results are above any other results since only out-of-plane displcement boundary conditons are imposed along the skewed boundary lines of the semi-infinite plate. For simply supported-clamped and clamped boundary conditions, the results from the present formulation are in good agreement with VICON since the clamped boundary conditions on the skewed edges

Table 8 Buckling coefficient K for simply supported-clamped anisotropic skewed plates $[45/90/-45]_s$ laminate

Load case	VICON	STAGS	Present analysis
		$\psi = 30$ deg	
B	1.976	1.967	1.973
C	2.388	2.374	2.381
D	2.942	2.915	2.923
		$\psi = 45$ deg	
B	2.857	2.832	2.872
C	3.480	3.450	3.505
D	4.360	4.327	4.407

Table 9 Buckling coefficient K for clamped anisotropic skewed plates $[\pm 45/90/0]_s$ laminate

Load case	VICON	STAGS	Present analysis
		$\psi = 30$ deg	
B	6.134	6.090	6.126
C	7.043	6.988	7.019
D	7.717	7.657	7.680
		$\psi = 45$ deg	
B	8.743	8.629	8.737
C	10.154	10.008	10.121
D	11.273	11.812	11.302

Table 10 Buckling coefficient K for clamped anisotropic skewed plates $[45/90/-45]_s$ laminate

Load case	VICON	STAGS	Present analysis
		$\psi = 30$ deg	
B	3.783	3.765	3.784
C	4.590	4.576	4.589
D	5.453	5.436	5.440
		$\psi = 45$ deg	
B	5.617	5.478	5.602
C	6.850	6.807	6.850
D	8.107	8.083	8.106

Table 11 Buckling coefficient K for clamped skewed plates with different thickness-to-width ratio

t/b	Isotropic	Laminate 1	Laminate 2
		$\psi = 30$ deg	
0.001	7.138	7.680	5.440
0.010	7.117	7.596	5.382
0.100	5.970	3.868	2.727
		$\psi = 45$ deg	
0.001	10.601	11.302	8.106
0.010	10.525	11.106	7.972
0.100	6.719	4.636	3.299

for these cases can be approximately easily. The STAGS results compare very well with those of the present formulation, especially for simply supported-clamped and clamped boundary conditions. Increasing degree of anisotropy has more effect on the buckling coefficients for positive shear loading conditions.

Effect of Transverse-Shear Deformation

The effect of transverse deformation is studied by considering isotropic and anisotropic skewed plates with different thickness-to-width ratios t/b for a plate aspect ratio (a/b) of 1. Clamped boundary conditions are considered, and the plates are subjected to load case D.

The present analysis results obtained using a 78-term series solution are shown in Table 11. Considering the isotropic plate, the buckling coefficients for $t/b = 0.001$ and 0.01 differs by less than 1% for both skew angles considered. As the plate thickness increases

($t/b = 0.1$), a significant decrease in the value of the buckling coefficients occurs due to shear flexibility. The buckling coefficients for the $t/b = 0.1$ case are reduced by 16 and 36% compared to the $t/b = 0.001$ case for skew angles of 30 and 45 deg, respectively. These results indicate that transverse shear effects become more important as the thickness increases and as the skew angle increases.

For anisotropic plates, the buckling coefficients for plate thickness to width ratio (t/b) = 0.001 and 0.01 differs by less than 2% for both skew angles and both laminates as shown in Table 11. As the plate thickness increases further ($t/b = 0.1$), a significant decrease in the value of buckling coefficient occurs. For both laminates, this decrease is 49 and 59% compared to the $t/b = 0.01$ case for skew angles of 30 and 45 deg, respectively. These results indicate that for laminated anisotropic plates the buckling coefficient is significantly reduced as the thickness or skew angle increases. For the 30-deg case, the change in buckling coefficient for $t/b = 0.01$ to $t/b = 0.1$ for anisotropic plates is nearly three times that for the isotropic plate. As the skew angle increases, the difference between isotropic and anisotropic plates decreases.

Therefore, the size of the skew angle significantly affects the buckling response of thick skewed plates. The percentage decrease for laminate 1 and laminate 2 is more than that for isotropic plate since laminated composites have low-shear modulus compared to isotropic material.

Concluding Remarks

A Rayleigh–Ritz method combined with a variational formulation and a first-order transverse-shear-deformation theory has been presented for buckling of arbitrary quadrilateral plates with various boundary conditions and subjected to combined in-plane loading. The Ritz functions consist of polynomials which include circulation functions to impose various boundary conditions. Numerical results are obtained for isotropic, orthotropic, and anisotropic plates with skewed geometries. The present analysis method does not exhibit any mesh distortion sensitivity, accurately models parallelogram-shaped geometries, accounts for material anisotropy, and can accommodate combined loading conditions.

The sensitivity of the buckling coefficient to the direction of the in-plane shear prestress application is studied for increasing skew angles. The influence of the skew angle on the buckling coefficient is more pronounced as the skew angle increases for thin plates as well as thick plates. The results also suggest that material anisotropy accentuates this effect. For the analysis cases studied in this paper, the present formulation provides accurate buckling results for skewed isotropic and anisotropic plates which will be useful in the preliminary design of stiffened structures.

Acknowledgment

The work of the first two authors was supported by NASA Contract NAS1-19858, Task No. 21, and is gratefully acknowledged.

References

[1]Ambur, D. R., and Rehfield, L. W., "Effect of Stiffness Characteristics on the Response of Composite Grid-Stiffened Structures," *Proceedings of the AIAA/ASME/ASCE/AHS/ASC 32nd Structures, Structural Dynamics, and Materials Conference*, (Baltimore, MD), Pt. 2, AIAA, Washington, DC, 1991, pp. 1349–1356 (AIAA Paper 91-1087).

[2]Jaunky, N., "Elastic Buckling of Stiffened Composite Curved Panel," Master's Thesis, Old Dominion Univ., Norfolk, VA, Aug. 1992.

[3]Phillips, J. L., and Gurdal, Z., "Structural Analysis and Optimum Design of Geodesically Stiffened Composite Panels," Center for Composite Materials and Structures, Rept. CCMS-90-05, Virginia Polytechnic Inst. and State Univ., Blacksburg, VA, July 1990.

[4]Wang, C. M., Liew, K. M., and Alwis, W. A. M., "Buckling of Skew Plates and Corner Condition for Simply Supported Edges," *ASCE Journals of Engineering Mechanics Division*, Vol. 118, No. 4, 1992, pp. 651–662.

[5]Smith, J. P., "General Plate Stability using High Order Techniques," *Proceedings of the AIAA/ASME/ASCE/AHS/ASC 33rd Structures, Structural Dynamics, and Materials Conference*, (Dallas, TX), Pt. 1, AIAA, Washington, DC, 1992, pp. 230–240 (AIAA Paper 92-2283).

[6]Smith, J. P., "BUCKY—A Finite Element Program for Plate p-Analysis," *Proceedings of the AIAA/ASME/ASCE/AHS/ASC 35th Structures, Structural Dynamics, and Materials Conference*, (Hilton Head, SC), Pt. 2, AIAA, Washington, DC, 1994, pp. 694–702 (AIAA Paper 94-1391).

[7]Jaunky, N., Knight, N. F., Jr., and Ambur, D. R., "Buckling of Arbitrary Quadrilateral Anisotropic Plates," *Proceedings of the 35th Structures, Structural Dynamics, and Materials Conference*, (Hilton Head, SC), Pt. 1, AIAA, Washington, DC, 1994, pp. 493–503 (AIAA Paper 94-1369).

[8]Singh, B., and Chakraverty, S., "Transverse Vibration of Plates using Characteristic Orthogonal Polynomials in Two Variables," *International Journal of Mechanical Sciences*, Vol. 34, No. 12, 1992, pp. 947–955.

[9]Stein, M., and Neff, J., "Buckling Stresses of Simply Supported Rectangular Flat Panels in Shear," NACA TN 1222, March 1947.

[10]Almroth, B. O., Brogan, F. A., and Stanley, G. M., "Structural Analysis of General Shells—User Instructions for STAGSC-1," Rept. LMSC-D633873, Lockheed Palo Alto Research Lab., Palo Alto, CA, Dec. 1982.

[11]Aminpour, M. A., "An Assumed-Stress Hybrid 4-Node Shell Element with Drilling Degrees of Freedom," *International Journal for Numerical Methods in Engineering*, Vol. 33, No. 1, 1992, pp. 19–38.

[12]Williams, F. W., Anderson, M. S., Kennedy, D., Butler, R., Aston, G., and Hoh, S. M., "An Exact Analysis and Optimum Design Program Covering the Buckling and Vibration of Prismatic Assemblies of Flat In-Plane Loaded, Anisotropic Plates, with Approximations for Curved and Tapered Plates, Discrete Supports and Transverse Stiffeners—User Manual for VICONOPT," NASA CR-181966, Release 1.2, Jan. 1993.

[13]Wittrick, W. H., "Buckling of Oblique Plates with Clamped Edges under Uniform Compression," *Aeronautical Quarterly*, Vol. 4, Feb. 1953, pp. 151–163.

[14]Durvasula, S., "Buckling of Clamped Skew Plates," *AIAA Journal*, Vol. 8, No. 1, 1970, pp. 178–181.

[15]Kitipornchai, S., Xiang, L., Wang, C. M., and Liew, K. M., "Buckling of Thick Skew Plates," *International Journal for Numerical Method in Engineering*, Vol. 36, No. 8, 1993, pp. 1299–1310.

[16]Fried, I., and Schmitt, K. H., "Numerical Results from the Application of Gradient Iterative Techniques to the Finite Element Vibration and Stability Analysis of Skew Plates," *Aeronautical Journal*, Vol. 76, March 1972, pp. 166–169.

[17]Edwardes, R. J., and Kabaila, A. P., "Buckling of Simply Supported Skew Plates," *International Journal for Numerical Methods in Engineering*, Vol. 12, No. 5, 1978, pp. 779–785.

[18]Mizusawa, T., Kajita, T., and Naruko, M., "Analysis of Skew Plate Problems with Various Constraints," *Journal of Sound and Vibration*, Vol. 73, No. 4, 1980, pp. 575–584.

[19]Kennedy, J. B., and Prabhakara, M. K., "Combined-Load Buckling of Orthotropic Skew Plates," *ASCE Journal of the Engineering Mechanics Division*, Vol. 105, No. EM1, 1979, pp. 71–79.

[20]Green, A. E., "Double Fourier Series and Boundary Value Problems," *Proceeding of the Cambridge Philosophical Society*, Vol. 40, Oct. 1944, pp. 222–228.